Pattern Formation in the Brusselator System on Fixed, Growing, and Contracting Domains

B5.5 Further Mathematical Biology

Jake Bowhay

Abstract

In this report, we study Turing instabilities in an abstract trimolecular reaction called the Brusselator. A system of reaction-diffusion partial differential equations (PDEs) modelling this chemical reaction is derived. The conditions for a Turing instability are derived using linear stability analysis. Following [14], a Lagrangian transformation is used to allow the system to be studied on a domain that is uniformly and isotropically deformed in time. To verify the validity of the linear stability analysis and understand the system's dynamic on a deforming domain, we present a numerical scheme for solving reaction-diffusion systems. Finally, using this scheme, we present numerical results for the Brusselator on a fixed, growing, and, rarely studied, contracting one-dimensional domain. These results show the presence of pattern formation on a fixed domain. For growing domains, we find that the pattern undergoes period doubling via peak splitting, as reported by [4], whereas on a contracting domain the period halving occurs by the peaks terminating rather than recombining.

1 Introduction

Turing's 1952 seminal paper "The chemical basis of morphogenesis" [25] showed that it was possible for simple reaction-diffusion equations to undergo a so-called Turing instability leading to the formation of spatially heterogeneous patterns. This result showed that a spatially homogeneous equilibrium that is stable in the absence of diffusion can be driven to instability with the addition of diffusion. This is a surprising result as diffusion is usually considered to be stabilising due to its smoothing nature. However, in the case of a Turing instability the interaction between the diffusion and reaction terms leads to complex dynamics, which has led to a wide range of research into reaction-diffusion equations.

The motivation for Turing's work came from the study of morphogenesis, which is the process by which cells differentiate from each other. This involves chemical morphogens which react together and diffuse through tissue, affecting the morphogenesis process. Turing showed that a system containing two morphogens could emit spatially heterogeneous patterns in the concentration of the morphogens and hypothesised these patterns might explain spatial organisation in embryos. Subsequently, these ideas have also been applied to a wide range of areas such as the patterning of teeth in alligators [12], stripe formation in juvenile Pomacanthus [20], and mutant mouse limbs [16]. However, Turing's work is not without its criticism as no

real morphogens have been found [8] and because the resulting patterns formed lack robustness to changes in the initial conditions [4]. Despite this, there have been multiple chemical reactions that have experimentally exhibited the pattern formation predicted by Turing's theory [19, 13].

Turing's original work considered a fixed domain, however, during biological processes such as embryonic development this may no longer be a good assumption. Crampin et al. [4] investigate the effect of slow isotropic growth in one dimension and suggest that domain growth could be a mechanism for robust pattern formation. In this report, we reproduce this result and extend it to the case of domain contraction. In their subsequent paper [5], Crampin et al. investigate non-uniform domain growth and show this leads to patterns not seen during uniform domain growth, however, this is beyond the scope of this report.

2 The Brusselator

Prigogine and Nicolis conceived the Brusselator system [21] in 1985 as an abstract trimolecular reaction which can exhibit chemical oscillations. It describes a reaction which turns two initial substances, A and B, into two products, D and E, via two intermediary substances X and Y. The four stages of the reaction are given by

$$A \xrightarrow{k_1} X, \tag{1}$$

$$2X + Y \xrightarrow{k_2} 3X, \tag{2}$$

$$B + X \xrightarrow{k_3} Y + D, \tag{3}$$

$$X \xrightarrow{k_4} E, \tag{4}$$

where k_1, k_2, k_3, and k_4 are the rates of reaction for each stage. We assume there is a sufficiently large quantity of the initial reactants A and B such that their concentrations can be considered positive constants. Applying the law of mass action [17] to reactions (1)-(4) yields the following system of ordinary differential equations (ODEs)

$$\frac{\mathrm{d}X}{\mathrm{d}t} = k_1 A + k_2 X^2 Y - k_3 B X - k_4 X, \tag{5}$$

$$\frac{\mathrm{d}Y}{\mathrm{d}t} = -k_2 X^2 Y + k_3 B X, \tag{6}$$

$$\frac{\mathrm{d}D}{\mathrm{d}t} = k_3 B X, \tag{7}$$

$$\frac{\mathrm{d}E}{\mathrm{d}t} = k_4 X, \tag{8}$$

where each variable denotes the concentration of the corresponding chemical. Here we note that (7) and (8) are decoupled from the rest of the system and subsequently will be omitted from further analysis.

Next, we seek to non-dimensonalise equations (5) and (6) by introducing the following dimensionless variables

$$u = \sqrt{\frac{k_2}{k_4}}X, \quad v = \sqrt{\frac{k_2}{k_4}}Y, \quad \text{and} \quad \tilde{t} = k_4 t. \tag{9}$$

We also introduce the following dimensionless parameter groupings

$$a = \frac{Ak_1}{k_4\sqrt{\frac{k_4}{k_2}}}, \quad \text{and} \quad b = \frac{Bk_3}{k_4}. \tag{10}$$

Substituting these into (5) and (6) gives

$$\frac{\mathrm{d}u}{\mathrm{d}\tilde{t}} = a - (b+1)u + u^2 v, \tag{11}$$

$$\frac{\mathrm{d}v}{\mathrm{d}\tilde{t}} = bu - u^2 v. \tag{12}$$

This is similar to the commonly studied Schnakenberg model [23]. Note, from here onwards, for notational convenience, we drop $\tilde{t}$ and let t denote the dimensionless time. Finally, we relax the assumption that the chemicals are well mixed and apply Fick's second law of diffusion [24] to get

$$\frac{\partial u}{\partial t} = \nabla^2 u + a - (b+1)u + u^2 v = \nabla^2 u + f(u,v), \tag{13}$$

$$\frac{\partial v}{\partial t} = D\nabla^2 v + bu - u^2 v = D\nabla^2 v + g(u,v), \tag{14}$$

where D is a dimensionless coefficient that captures the ratio of diffusivity of B compared to the diffusivity of A. This takes the standard form of a reaction-diffusion equation given by (15).

3 Conditions for Pattern Formation

In this section, we will derive the necessary conditions for a Turing instability to occur in a reaction-diffusion system of two chemicals. The reaction and diffusion of these two chemical concentrations $u(\mathbf{x}, t)$ and $v(\mathbf{x}, t)$ is modelled by the coupled PDEs

$$\frac{\partial \mathbf{u}}{\partial t} = \mathcal{D}\nabla^2 \mathbf{u} + \mathcal{R}(\mathbf{u}), \qquad \mathbf{x} \in \Omega,\ t > 0, \tag{15}$$

where Ω is an open, bounded, and connected domain and

$$\mathbf{u} = \begin{pmatrix} u(\mathbf{x},t) \\ v(\mathbf{x},t) \end{pmatrix}, \quad \mathcal{D} = \begin{pmatrix} D_u & 0 \\ 0 & D_v \end{pmatrix}, \quad \text{and} \quad \mathcal{R}(\mathbf{u}) = \begin{pmatrix} f(\mathbf{u}) \\ g(\mathbf{u}) \end{pmatrix},$$

with specified initial conditions $\mathbf{u}(\mathbf{x},0)$. We will assume homogeneous Neumann boundary conditions $\mathbf{n}\cdot\nabla\mathbf{u} = 0$ on $\partial\Omega$, where $\mathbf{n}$ is the outwards facing unit normal to the boundary of the domain $\partial\Omega$. This is a natural choice as it implies there is no external input to the system and hence any pattern formation is caused by phenomena inherent to the system itself rather than a flux-driven instability.

Definition 1 (Turing Instability)**.** *A reaction-diffusion system exhibits a Turing instability if, for the well-mixed case (in the absence of diffusion), there is a spatially homogeneous, asymptotically stable steady state which becomes unstable in the presence of diffusion [17].*

3.1 Well Mixed Stability

We proceed in a similar fashion to Murray [17] and first look for conditions for which the well-mixed system ($D_u = D_v = 0$) has an asymptotically stable homogeneous steady state $\mathbf{u}^*$. That is $f(\mathbf{u}^*) = g(\mathbf{u}^*) = 0$. We then proceed to linearise about the steady state by considering the perturbed steady state $\mathbf{u} = \mathbf{u}^* + \boldsymbol{\xi}$, where $\|\boldsymbol{\xi}\| \ll 1$. Hence by Taylor expansion of (15) about the steady state and neglecting higher order terms, we have

$$\frac{\partial \boldsymbol{\xi}}{\partial t} = \left.\begin{pmatrix} f_u & f_v \\ g_u & g_v \end{pmatrix}\right|_{\mathbf{u}^*} \boldsymbol{\xi} = \mathbf{J}\boldsymbol{\xi}, \tag{16}$$

where $\mathbf{J}$ is the Jacobian matrix evaluated at $\mathbf{u}^*$. The solution of (16), assuming $\mathbf{J}$ is semi-simple, is given by $\boldsymbol{\xi}(\mathbf{x},t) = \boldsymbol{\xi}(\mathbf{x},0)\exp(\mathbf{J}t) = \boldsymbol{\xi}(\mathbf{x},0)\mathbf{V}\,\mathrm{diag}(\exp(\lambda_1 t),\exp(\lambda_2 t))\mathbf{V}^{-1}$ where $\mathbf{V}$ is the matrix of eigenvectors and λ_i the eigenvalues of $\mathbf{J}$. Thus, for the steady state $\boldsymbol{\xi} = 0$ of the linearised system (16) to be asymptotically stable, we require $\Re(\lambda_i) < 0$ for $i = 1, 2$. If this is satisfied, by the Hartman–Grobman theorem [9], the non-linear system without diffusion is also asymptotically stable in a neighbourhood of the equilibrium $\mathbf{u}^*$. The eigenvalues of $\mathbf{J}$ are given by

$$\lambda_{1,2} = \frac{1}{2}\left(\mathrm{Tr}(\mathbf{J}) \pm \sqrt{(\mathrm{Tr}(\mathbf{J}))^2 - 4\det(\mathbf{J})}\right), \tag{17}$$

and hence asymptotic stability in the absence of diffusion is guaranteed if both of the following conditions hold:

Condition 1. $\mathrm{Tr}(\mathbf{J}) = f_u + g_v < 0$,

Condition 2. $\det(\mathbf{J}) = f_u g_v - f_v g_u > 0$.

3.2 Instability in the Presence of Diffusion

Performing the same Taylor expansion as previous, this time in the presence of diffusion, leads to the full linearised system

$$\frac{\partial \boldsymbol{\xi}}{\partial t} = \mathcal{D}\nabla^2 \boldsymbol{\xi} + \mathbf{J}\boldsymbol{\xi}. \tag{18}$$

We then assume a separable solution ansatz given by $\boldsymbol{\xi}(\mathbf{x}, t) = T(t)\mathbf{w}(\mathbf{x})$. Substituting this into (18) and rearranging it into a separated form gives

$$\frac{\mathrm{d}T}{\mathrm{d}t}\frac{1}{T}\mathbf{w} = \mathcal{D}\nabla^2\mathbf{w} + \mathbf{J}\mathbf{w}. \tag{19}$$

We note that the terms in T are independent of space and the right-hand side is independent of time. Hence, we have

$$\frac{\mathrm{d}T}{\mathrm{d}t} = \lambda T, \tag{20}$$

where λ is the eigenvalue of the system in the presence of diffusion. Thus $T = T_0 \exp(\lambda t)$ for some non-zero constant T_0. The temporal growth or decay and consequently the stability of the solution is therefore determined by λ. We also have the following equation for $\mathbf{w}$

$$\mathcal{D}\nabla^2\mathbf{w} + \mathbf{J}\mathbf{w} = \lambda\mathbf{w}, \tag{21}$$

with homogeneous Neumann boundary conditions $\mathbf{n} \cdot \nabla\mathbf{u} = 0$ on $\partial\Omega$ as before. On an open, bounded, and connected domain, the Laplace operator has discrete non-negative eigenvalues [7]. Hence, we assume an eigenfunction expansion of $\mathbf{w}$ such that

$$\mathbf{w}(\mathbf{x}) = \sum_k \mathbf{c}_k w_k(\mathbf{x}). \tag{22}$$

On rectangle-like cartesian product domains with Neumann boundary conditions, we can assume a separable solution for $w_k(x)$ which yields cosine terms [7]. From this, the following relation holds $\nabla^2\mathbf{w} = -k^2\mathbf{w}$, where k is the wavenumber. Thus, (21) can be rewritten as

$$\left[\lambda\mathbf{I} - \mathbf{J} + \mathcal{D}k^2\right]\mathbf{w} = 0. \tag{23}$$

For non-trivial solutions of $\mathbf{w}$ to exist, we must have

$$\det(\lambda\mathbf{I} - \mathbf{J} + \mathcal{D}k^2) = 0, \tag{24}$$

or equivalently

$$\lambda^2 + \lambda\left[k^2\left(D_u + D_v\right) - \left(f_u + g_v\right)\right] + h(k^2) = 0, \tag{25}$$

$$h(k^2) = D_u D_v k^4 - (D_v f_u + D_u g_v)\, k^2 + \det(\mathbf{J}). \tag{26}$$

For instability in the presence of diffusion we require that, for at least one of the eigenvalues, $\Re(\lambda\,(k^2)) > 0$. From condition 1 we require $f_u + g_v < 0$ and as $D_u, D_v > 0$ the coefficient of λ in (25) must be positive. Consequently, to satisfy $\Re(\lambda(k^2)) > 0$, we require that $h(k^2) < 0$. Condition 2 dictates that $\det(\mathbf{J}) > 0$ and as $D_u, D_v > 0$, a necessary condition for $h(k^2) < 0$ is

Condition 3. $D_v f_u + D_u g_v > 0$.

A corollary to condition 1 and condition 3 is that for these two conditions to hold simultaneously we must have $D_u \neq D_v$ and also $\text{sign}(f_u) \neq \text{sign}(g_v)$. To derive a sufficient condition for $\Re(\lambda(k^2)) > 0$ we solve ${}^{\mathrm{d}h}/_{\mathrm{d}(k^2)} = 0$ which gives the minimiser

$$(k^*)^2 = \frac{D_v f_u + D_u g_v}{2 D_u D_v}, \tag{27}$$

at which we have

$$h\left((k^*)^2\right) = \det(\mathbf{J}) - \frac{(D_v f_u + D_u g_v)^2}{4 D_u D_v}. \tag{28}$$

As we require $h(k^2) < 0$, this provides the final condition for a Turing instability to occur:

Condition 4. $\det(\mathbf{J}) < \frac{(D_v f_u + D_u g_v)^2}{4 D_u D_v}$.

3.3 Minimum Domain Size

The wavenumber k in the expansion (22) takes discrete values and therefore, whilst there might exist an interval of values of k such that $h(k^2) < 0$, the discrete values of k may not coincide with this interval. In this case, whilst the conditions for a Turing instability may be satisfied, there is no pattern formation.

In the 1D domain $\Omega = (0, L)$, the wavenumber is given by $k = {}^{n\pi}/_{L}$ where $n = 0, 1, 2, \ldots$ where n is the mode of the system. From (26) we know that to achieve $h(k^2) < 0$ we must have

$$k^2 \in \left[\frac{D_v f_u + D_u g_v - \sqrt{(D_v f_u + D_u g_v)^2 - 4 D_u D_v \det(\mathbf{J})}}{2 D_u D_v}, \right.$$
$$\left. \frac{D_v f_u + D_u g_v + \sqrt{(D_v f_u + D_u g_v)^2 - 4 D_u D_v \det(\mathbf{J})}}{2 D_u D_v} \right]. \tag{29}$$

Hence, we require L to be sufficiently large such that (29) holds for at least one non-zero value of n, giving an unstable wavenumber. This also reveals that as the domain size increases the pattern admitted becomes more complicated as the number of admissible unstable wavenumbers increases [15]. Whilst the linear stability analysis performed here would suggest that the modes associated with the admissible unstable wavenumbers would grow exponentially, in reality, the non-linearity we have ignored bounds their growth. This is shown by the numerical results in section 6.

3.4 Analysis of the Brusselator

In this section, we will apply the derived conditions 1–4 in a similar fashion to [2] in order to show that the Brusselator system is capable of undergoing a Turing instability. The homogeneous steady state of (13) and (14) is given by $\mathbf{u}^* = (a, b/a)$, as shown in fig. 1a. The Jacobian evaluated at $\mathbf{u}^*$ is given by

$$\mathbf{J} = \begin{pmatrix} b-1 & a^2 \\ -b & -a^2 \end{pmatrix}. \tag{30}$$

Hence, from conditions 1–4 we have

$$b - 1 - a^2 < 0, \tag{31}$$

$$a^2 b - a^2(b-1) = a^2 > 0, \tag{32}$$

$$D(b-1) - a^2 > 0, \tag{33}$$

$$\left(D(b-1) - a^2\right)^2 - 4Da^2 > 0. \tag{34}$$

We note that (32) is trivially satisfied for all non-zero parameter values so the stability of the well-mixed steady state is entirely determined by (31). From (31), when $b-1 = a^2$ the system undergoes a Hopf bifurcation meaning the stable equilibrium needed for a Turing instability becomes a limit cycle, as shown in fig. 1b, and a Turing instability is no longer possible. For both (1) and (3) to simultaneously be true we must have $D > 1$. The final condition (34) gives a inequality that is quadratic in b

$$D^2 b^2 - 2D\left(D + a^2\right) b + D^2 - 2Da^2 + a^4 > 0. \tag{35}$$

This is satisfied if either of the following inequalities hold

$$b < \frac{D + a^2 - 2a\sqrt{D}}{D}, \tag{36}$$

$$b > \frac{D + a^2 + 2a\sqrt{D}}{D}. \tag{37}$$

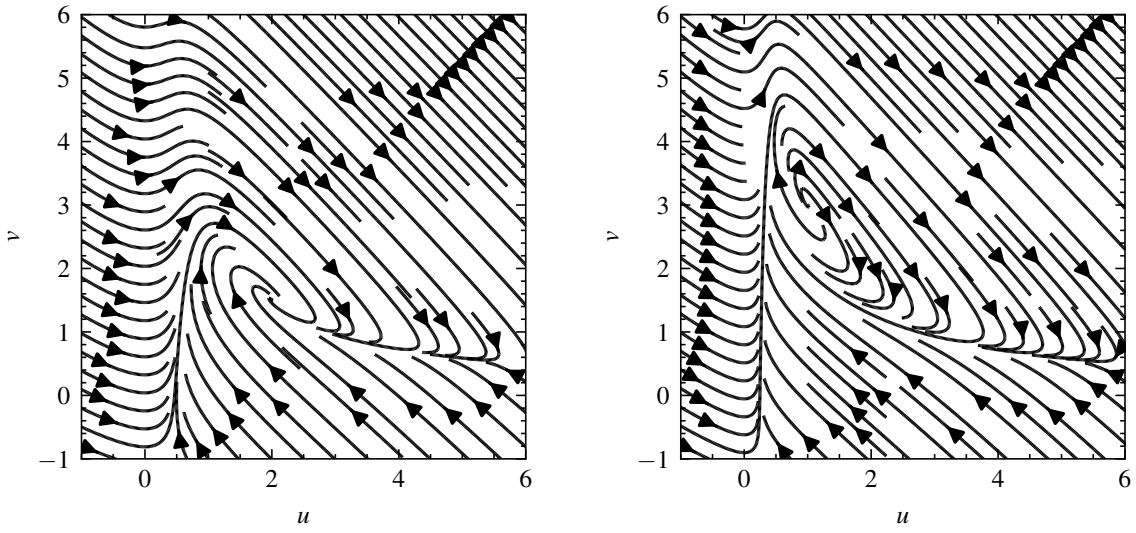

(a) Parameters $(a, b) = (2, 3)$, which shows a stable equilibrium at $\mathbf{u}^* = (1, 1.5)$ as predicted by (31).

(b) Parameters $(a, b) = (1, 3)$, which shows the existence of a stable limit cycle created by a Hopf bifurcation.

Figure 1: Phase portraits of the well-mixed Brusselator system.

The first inequality (36) contradicts (33) meaning they cannot simultaneously hold. If the second inequality (37) holds then (33) also holds, hence making (33) redundant. The two inequalities, (31) and (37), thereby define two bounding curves in the (a, b) parameter space that determines the so-called Turing space [18], as shown in fig. 2. From this, we note that as $D \to \infty$, the range of parameters for which a Turing instability is possible increases.

We can calculate the allowable wave numbers for a given length domain for the Brusselator system by applying (29), giving the allowable wave numbers as

$$k^2 \in \left[\frac{D\left(b-1\right) - a^2 - \sqrt{\left(D\left(b-1\right) - a^2\right)^2 - 4Da^2}}{2D}, \right.$$
$$\left. \frac{D\left(b-1\right) - a^2 + \sqrt{\left(D\left(b-1\right) - a^2\right)^2 - 4Da^2}}{2D} \right]. \quad (38)$$

The linear stability analysis can be applied to predict what might be the dominant wave number in the system. The mode n associated with the most positive $\Re(\lambda(k^2))$ grows the fastest and therefore is most likely to be dominant when the system enters the non-linear regime. The allowable and expected dominant wave modes for the parameter values $(D, a, b) = (20, 2, 3)$ as L increases are shown in fig. 3. As expected,

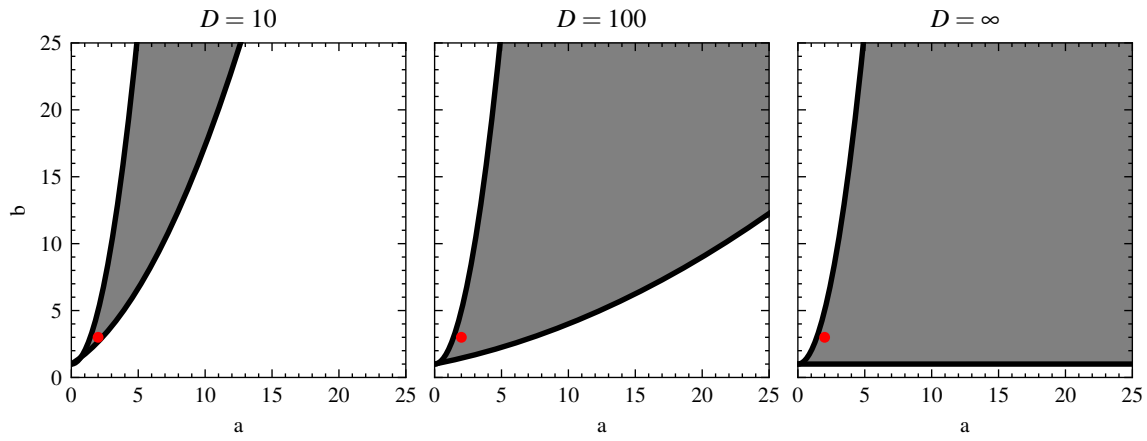

Figure 2: The Turing space for the Brusselator with varying values of D. The shaded area denotes where conditions 1–4 are satisfied. The red point denotes the parameter values $(a, b) = (2, 3)$, which are used in the forthcoming numerical simulations. This shows these are suitable parameter values to use for a Turing instability to occur.

increasing L leads to more admissible wave modes.

4 Pattern Formation on Changing Domains

In this section, we seek to extend (15) to allow for the possibility that the domain changes in time. A general two chemical reaction-diffusion equation on a changing one-dimensional domain takes the form

$$\frac{\partial u}{\partial t} + \frac{\partial}{\partial x}(au) = \frac{\partial^2 u}{\partial x^2} + f(u, v), \tag{39}$$

with an equivalent expression of v and where a is the velocity induced by the domain growth [4]. We then proceed in a similar fashion to Madzvamuse and Maini [14] and introduce a transformation between the growing domain and the fixed domain. The new Lagrangian coordinate in the growing domain which changes with time is given by

$$x = \hat{x}(\xi, t), \tag{40}$$

where $\xi \in [0, 1]$ is a fixed coordinate that does not change in time. The transformation maps the chemical concentrations to new functions $u(x, t) = \hat{u}(\xi, t)$ and $v(x, t) = \hat{v}(\xi, t)$. Then we define the material derivative as

$$\frac{\mathrm{D}\hat{u}}{\mathrm{D}t} \equiv \frac{\partial u}{\partial t} + \frac{\partial u}{\partial x}\frac{\partial x}{\partial t} \equiv \frac{\partial u}{\partial t} + a\frac{\partial u}{\partial x}, \tag{41}$$

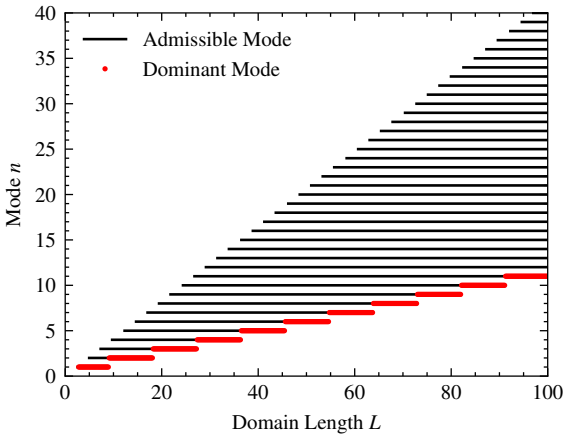

Figure 3: The admissible and dominant modes as predicted by the linear stability analysis for the Brusselator system as the domain length L increases for the parameter values $(D, a, b) = (20, 2, 3)$.

and, by the chain rule,

$$\frac{\partial u}{\partial x} = \frac{\partial \hat{u}}{\partial \xi}\frac{\partial \xi}{\partial x}. \tag{42}$$

It follows that the second derivative of u in space is then given by

$$\frac{\partial^2 u}{\partial x^2} = \frac{\partial^2 \hat{u}}{\partial \xi^2}\left(\frac{\partial \xi}{\partial x}\right)^2 + \frac{\partial \hat{u}}{\partial \xi}\frac{\partial^2 \xi}{\partial x^2} \tag{43}$$

The equivalent analysis can also be performed for v. Using (41) and (43) we can rewrite (39) for both $\hat{u}$ and $\hat{v}$ as

$$\frac{\mathrm{D}\hat{u}}{\mathrm{D}t} = \frac{\partial^2 \hat{u}}{\partial \xi^2}\left(\frac{\partial \xi}{\partial x}\right)^2 + \frac{\partial \hat{u}}{\partial \xi}\frac{\partial^2 \xi}{\partial x^2} + f(\hat{u}, \hat{v}) - \frac{\partial^2 x}{\partial x \partial t}\hat{u}, \tag{44}$$

$$\frac{\mathrm{D}\hat{v}}{\mathrm{D}t} = D\left(\frac{\partial^2 \hat{v}}{\partial \xi^2}\left(\frac{\partial \xi}{\partial x}\right)^2 + \frac{\partial \hat{v}}{\partial \xi}\frac{\partial^2 \xi}{\partial x^2}\right) + g(\hat{u}, \hat{v}) - \frac{\partial^2 x}{\partial x \partial t}\hat{v}. \tag{45}$$

For simplicity, we will only consider the case of uniform, isotropic growth. For non-uniform domain growth, we refer the interested reader to [5]. We let

$$\hat{x} = \rho(t)\xi, \tag{46}$$

where $\rho(t)$ is the growth function which controls how the domain changes in time. Hence, we have

$$\frac{\partial x}{\partial t} = \frac{\mathrm{d}\rho}{\mathrm{d}t}(t)\xi = \frac{x}{\rho(t)}\frac{\mathrm{d}\rho}{\mathrm{d}t}(t) \quad \Longrightarrow \quad \frac{\partial^2 x}{\partial x \partial t} = \frac{1}{\rho(t)}\frac{\mathrm{d}\rho}{\mathrm{d}t}(t), \tag{47}$$

$$\frac{\partial x}{\partial \xi} = \rho(t) \implies \left(\frac{\partial \xi}{\partial x}\right)^2 = \frac{1}{(\rho(t))^2}, \tag{48}$$

$$\frac{\partial^2 \xi}{\partial x^2} = 0, \tag{49}$$

which simplifies (44) and (45) to

$$\frac{\mathrm{D}\hat{u}}{\mathrm{D}t} = \frac{1}{(\rho(t))^2}\frac{\partial^2 \hat{u}}{\partial \xi^2} + f(\hat{u}, \hat{v}) - \frac{1}{\rho(t)}\frac{\mathrm{d}\rho}{\mathrm{d}t}(t)\hat{u}, \tag{50}$$

$$\frac{\mathrm{D}\hat{v}}{\mathrm{D}t} = \frac{D}{(\rho(t))^2}\frac{\partial^2 \hat{v}}{\partial \xi^2} + g(\hat{u}, \hat{v}) - \frac{1}{\rho(t)}\frac{\mathrm{d}\rho}{\mathrm{d}t}(t)\hat{v}. \tag{51}$$

We note that this transformation eliminates the advective term, which is advantageous as it simplifies the subsequent numerical scheme. In the case of slow growth $^{\mathrm{d}\rho}/_{\mathrm{d}t}$ is small so it is possible to omit the final term of both equations (50) and (51). However, for the numerical examples shown later this does not necessarily hold so the full form is used.

We consider three possible forms of domain growth, which are: linear growth given by

$$\rho(t) = L_0(1 + \gamma t), \tag{52}$$

exponential growth given by

$$\rho(t) = L_0 \exp(\gamma t), \tag{53}$$

and sinusoidal growth/contraction given by

$$\rho(t) = L_0 + \gamma \sin\left(\frac{2n\pi t}{T}\right), \tag{54}$$

where γ is a notional growth rate, L_0 is the initial domain size, n is the number of periods of growth/contraction, and T is the final time. For (52) and (53) the growth rate γ can be set to be negative for a contracting domain or to a piecewise continuous function of t for more interesting growth/contraction cases.

5 Numerical Scheme

To verify that the previously derived condition leads to a Turing instability and to investigate domain growth, we will solve the Brusselator system to a steady state on a 1D domain numerically. This will verify the presence of heterogeneous patterns in the full non-linear system, whereas in section 3 we relied on linear stability analysis, which is only valid in a neighbourhood of the equilibrium. The numerical scheme requires the problem to be discretised in time and space.

To solve (15) on the domain $\{(x,t) \in (0,L) \times [0,T]\}$, where $L > 0$ is the length of the domain and $T > 0$ is the final time, we first spatially discretise the problem using finite differences following [10]. We define a mesh by letting $N, M \in \mathbb{Z}^+$ be the number of steps in the spatial and temporal direction respectively. The spatial and temporal step-size is then given by $\Delta x = {}^{L}/_{N}$ and $\Delta t = {}^{T}/_{M}$. We then approximate the true solution $\mathbf{u}(x_i, t_m)$ by the numerical solution $\mathbf{U}_j^m$, where $x_j = j\Delta x$ for $j \in \{0, 1, \ldots, N\}$ and $t_m = m\Delta t$ for $m \in \{0, 1, \ldots, M\}$. The Laplacian term with homogeneous Neumann boundary conditions is then approximated by the second-order central difference operator given by

$$D_x^+ D_x^- \mathbf{U}_j^m = \begin{cases} \dfrac{2\mathbf{U}_{j+1}^m - 2\mathbf{U}_j^m}{(\Delta x)^2} & j = 0, \\ \dfrac{\mathbf{U}_{j+1}^m - 2\mathbf{U}_j^m + \mathbf{U}_{j-1}^m}{(\Delta x)^2} & 1 \leq j \leq N, \\ \dfrac{-2\mathbf{U}_j^m + 2\mathbf{U}_{j-1}^m}{(\Delta x)^2} & j = N. \end{cases} \tag{55}$$

This transforms (15) into a system of differential equations

$$\frac{\partial \mathbf{U}_j^m}{\partial t} = D_x^+ D_x^- \mathbf{U}_j^m + \mathcal{R}(\mathbf{U}_j^m), \tag{56}$$

which can then be integrated in time to find the solution.

Considerations for choosing the integration scheme for a reaction-diffusion system are discussed extensively by Ruuth [22]. Typically, the $D_x^+ D_x^- \mathbf{U}_j^m$ term is stiff meaning explicit schemes usually require prohibitively small timesteps. A fully implicit scheme can alleviate this restriction however inverting the nonlinear $\mathcal{R}(\mathbf{U}_j^m)$ term can be computationally difficult. Ruuth also highlights the importance of a scheme that strongly damps the error's high-frequency component, a property commonly used schemes such as Crank-Nicolson lack [22].

A common approach to avoid these issues is to use an implicit-explicit (IMEX) scheme, where we treat $D_x^+ D_x^- \mathbf{U}_j^m$ implicitly but $\mathcal{R}(\mathbf{U}_j^m)$ explicitly. When a second-order central difference is used for the diffusive term Ruuth recommends the use of the second-order semi-implicit backward differentiation formula (BDF) scheme, due to its strong decay of high-frequency error components [22, 1]. For our problem, this scheme is given by

$$\frac{1}{2\Delta t}\left(3\mathbf{U}_j^{m+1} - 4\mathbf{U}_j^m + \mathbf{U}_j^{m-1}\right) = \mathcal{D} D_x^+ D_x^- \mathbf{U}_j^{m+1} + 2\mathcal{R}(\mathbf{U}_j^m) - \mathcal{R}(\mathbf{U}_j^{m-1}). \tag{57}$$

The implicit part of the scheme leads to a tridiagonal linear system which can efficiently inverted using the Thomas algorithm. This scheme was also used to good

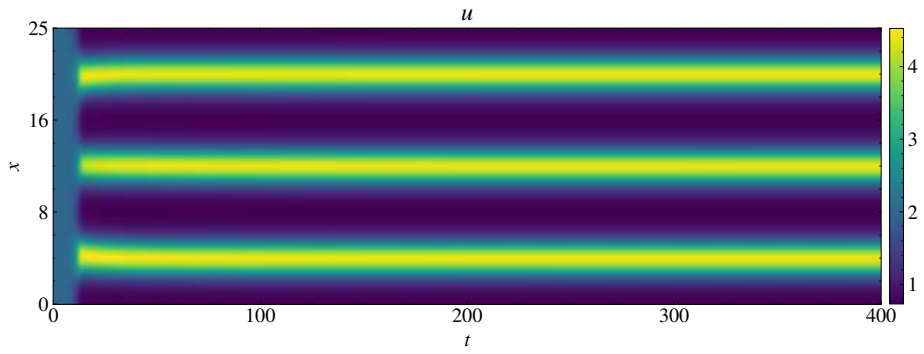

Figure 4: Numerical solution of the Brusselator exhibiting a Turing instability on a fixed domain of $L = 25$ with parameter values $(D, a, b) = (20, 2, 3)$. Here the dominant mode is $n = 6$.

effect in [2]. Since the scheme is a two-step method, we initially start the scheme with a single first-order semi-implicit BDF step given by

$$\frac{\mathbf{U}_j^{m+1} - \mathbf{U}_j^m}{\Delta t} = \mathcal{D} D_x^+ D_x^- \mathbf{U}_j^{m+1} + \mathcal{R}(\mathbf{U}_j^m). \tag{58}$$

We choose the initial data to be the well-mixed steady-state $(a, b/a)$ plus a small spatially varying random perturbation to induce diffusion.

6 Results

First, we compare the numerical results against the linear stability analysis for a fixed domain using the parameter values $(L, D, a, b) = (25, 20, 2, 3)$. From fig. 2 we know these parameter values satisfy conditions 1–4 as required for a Turing instability. The linear stability analysis, shown in fig. 3, predicts the dominant wave mode to be $n = 3$. The numerical results, as shown in fig. 4, show pattern formation as expected. The dominant wave mode after the transient dynamics of the system is $n = 6$ which, whilst one of the admissible wave modes, is not the dominant mode predicted by the linear stability analysis. In fact, for the same parameter values we can observe other dominant modes by using different random initial conditions, as shown in fig. 7 in appendix A. This phenomenon is also observed in [2]. This shows the limitations of the linear stability analysis when making predictions about the non-linear system and also the sensitivity of the dominant mode to the initial conditions. For brevity, we only report the value of u however v exhibits similar behaviour but is spatially antiphase to u.

Next, we consider an exponentially growing domain, given by the growth function (53), the numerical results of which are shown in fig. 5b. Crampin et al. [4] predicted by a self-similarity argument, that for exponential growth, the spatial pattern will undergo a frequency doubling when the domain doubles in length. In fig. 5b we see that the numerical results agree with this prediction as the first frequency doubling occurs at $x = 41$ and the second at $x = 82$. The mechanism for frequency doubling depends on the reaction kinetics: for the Schnakenberg system Crampin et al. observe peak splitting, whereas, for the Gierer-Meinhardt system, they observe peak insertion [4]. Which of the mechanisms occur depends on the non-linear reaction terms. For the Brusselator system, fig. 5b shows that frequency doubling occurs through peak splitting. It is perhaps not surprising that the two systems share similar dynamics as the Schakenberg system has a similar reaction term to the Brusselator.

We also consider the possibility of linear domain growth, as given by (18). The numerical results of which are shown in fig. 5a. Again, we observe that the pattern undergoes frequency doubling by peak splitting. Crampin et al. show that frequency doubling is not a natural consequence of linear domain growth so we would expect that, for a longer time scale, the observed frequency doubling would break down [4]. However, in contrast to the exponential growth, we observe that frequency doubling occurs close to but not exactly when the domain doubles in length. For example, in fig. 5a the first frequency doubling occurs at $x = 58$ and the second at $x = 112$, slightly under twice the length at which the first frequency doubling occurred at. Again, the mechanism for frequency doubling is peak splitting.

Inspired by [27], we then extend the case of linear and exponential domain growth by considering a change of sign in the growth rate γ so that the domain initially grows before contracting to return to its original starting size. This is shown in fig. 6a and fig. 6b. Whilst harder to motivate biologically, this leads to interesting dynamics that have not been widely studied in the literature. As before, when the domain grows the usual frequency doubling through peak splitting phenomena is observed. When the domain contacts, as one might expect, we observe frequency halving. However in contrast, when the domain is contracting, the frequency halving occurs through a mechanism we term *peak termination* and not the analogous peak recombining. This is qualitatively the reverse of the peak insertion behaviour that occurs in the Gierer-Meinhart system. Further work is required to establish if this peak termination occurs with other reactant terms such as the Gierer-Meinhart system or whether this behaviour is unique to the Brusselator (and other similar systems). At this point, one might be tempted to apply the linear stability analysis performed in section 3.3

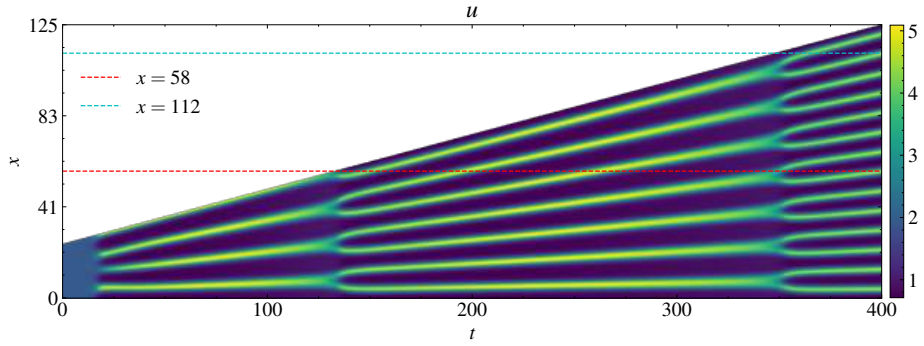

(a) Linearly domain growth given by (52), with $\gamma = 0.01$.

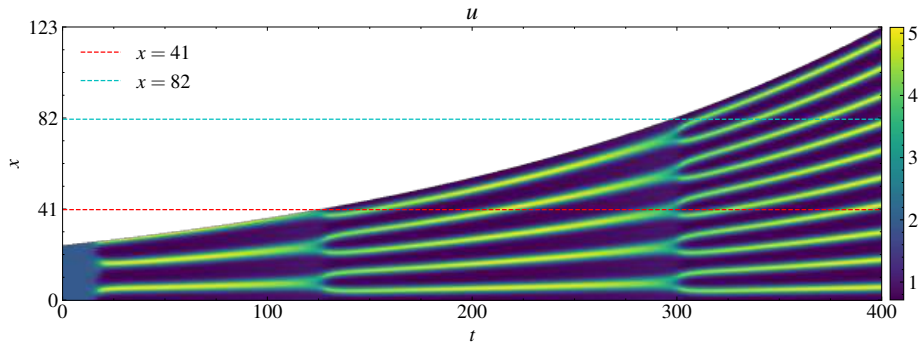

(b) Exponential domain growth given by (53), with $\gamma = 0.004$.

Figure 5: Numerical results of the Brusselator system on growing domains with parameter values $(D, a, b, L_0) = (20, 2, 3, 25)$. For both types of growth, we observe period doubling through peak splitting. The dashed line indicates the size of the domain at which peak splitting occurs.

to explain this behaviour through a wave number that becomes inadmissible as the domain shrinks. However, this behaviour occurs far from the steady state, in the non-linear regime where this linear stability analysis is no longer valid. Furthermore, if this was the case one would expect that frequency doubling and halving would occur at the same domain size but in fig. 6 we see that this is not the case. That said, it is clear that there is a sudden change in the dominant mode which is caused by the change in domain size.

It is also noteworthy that in all three examples shown in fig. 6 there is an asymmetry in the domain size at which the peak splitting and peak termination occur. In all cases investigated, the peak termination occurs at a smaller domain length than the respective splitting. This shows the pattern can persist on domain lengths smaller than the length it was created at.

Finally, we consider the case of a domain that repeatedly grows and shrinks, in

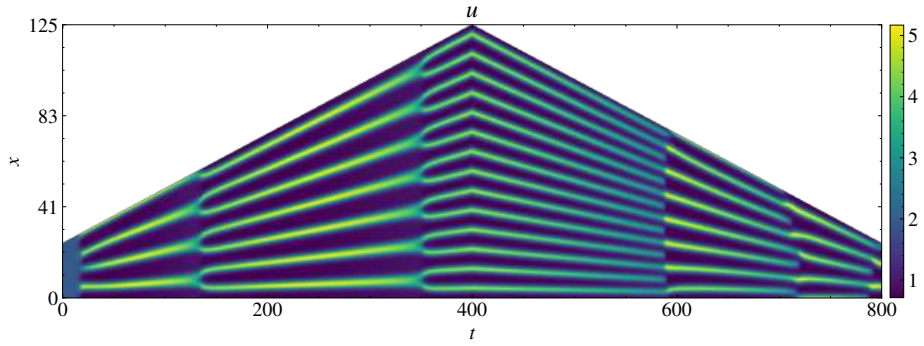

(a) Linear domain growth and contraction with parameters $(L_0, \gamma) = (25, \pm 0.01)$.

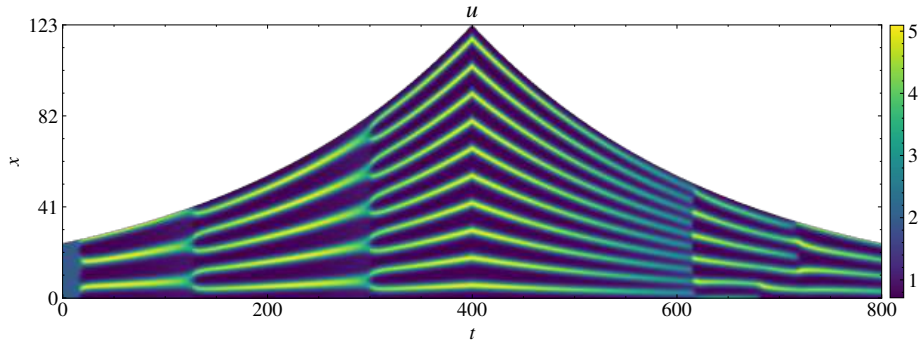

(b) Exponential domain growth and contraction with parameters $(L_0, \gamma) = (25, \pm 0.004)$.

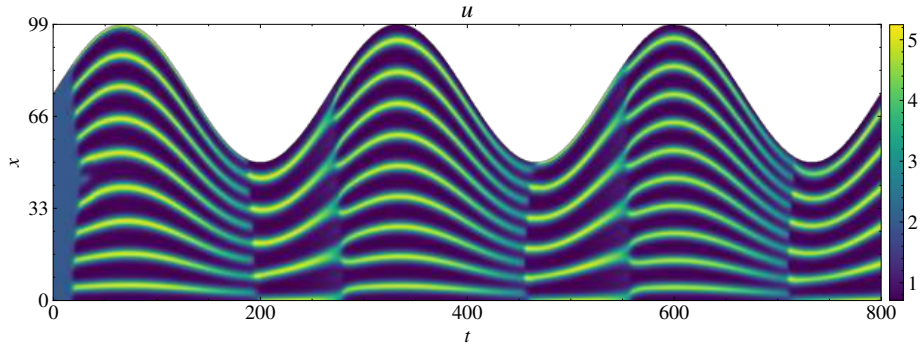

(c) Sinusoidal domain growth and contraction given by (54) with parameters $(L_0, \gamma, n) = (75, 25, 3)$.

Figure 6: Numerical results of the Brusselator system with growing and contracting domains with parameter values $(D, a, b) = (20, 2, 3)$.

this case in a sinusoidal fashion, as shown in fig. 6c. Here we observe a repeated frequency doubling, followed by frequency halving. As before, the frequency doubling occurs by peak splitting and the frequency halving occurs through peak termination. We see this behaviour occurs in every period, at the same domain size.

7 Discussion

The results in fig. 4 and fig. 7 demonstrate how identical systems with identical parameter values can exhibit different modes as a result of small changes to the initial conditions. The inability to reliably select the same pattern under expected random biological variations in the chemical concentrations (the model initial conditions) is potentially problematic in the application of Turing's theory [4]. Domain growth thereby plays an important role in creating so-called robustness. This is because, between frequency doublings, the pattern remains unchanged despite the changing domain size.

It is possible to extend the results shown in this report to non-uniform domain growth, as demonstrated in [5]. However, there appears to be very little work investigating non-uniform domain contraction so further research is required to determine if the peak termination we have reported also occurs in the case of non-uniform contraction. However, arguably more relevant to developmental biology is when the evolution of the domain is concentration-driven, as explored in [11]. They note that frequency doubling typically still occurs for slow growth however fast concentration-dependent evolution and domain contraction leads to unexpected behaviour. Hence, developing a better theoretical understanding of the results we have reported for contracting domains could help to enhance the understand of this behaviour.

Whilst contracting domains are harder to biologically motivate when compared to domain growth, there has been recent interest in the application of reaction-diffusion models to vegetation patterning [6]. In these models, it could be possible to justify a contracting domain due to human activity or ecological changes so understanding the effects of a contracting domain could provide additional insight. However, one current barrier to this application is the observed sudden termination of peaks as the domain shrinks is not representative of a slow process like vegetation growth. Further investigation would be needed to determine if the equivalent of peak termination occurs in two dimensions and whether the reaction terms used in vegetation models exhibit this mechanism of frequency halving.

In this report, we have only considered the Turing instability as a mechanism for pattern formation however current literature is beginning to look beyond at other mechanisms which produce localised patterns. For example, in their review paper, Champneys et al. highlight three additional mechanisms for pattern formation beyond the Turing instability [3]. These are Maxwell fronts, wave pinning and homoclinic snaking. For example, it has been shown that it is possible for homoclinic snaking

to occur in the Brusselator system [26]. However, so far there has been little work to consider the effect of a changing domain on these localised structures.

8 Conclusion

In this report, we have reproduced the necessary conditions for a Turing instability in a two-chemical system and have shown both analytically and numerically that the Brusselator system is capable of undergoing a Turing instability. Through the use of a Lagrangian transform, growing domains were investigated and a frequency doubling pattern was found in agreement with previous literature [4]. Finally, we showed that on domains that both grow and contract, there is an asymmetry between both the mechanism and location at which the frequency doubling/halving pattern takes place. Further work is required to understand why, in the Brusselator system, frequency doubling occurs by peak splitting but frequency halving occurs by peak termination and why these are not triggered at the same domain size.

Appendices

A Additional Figures

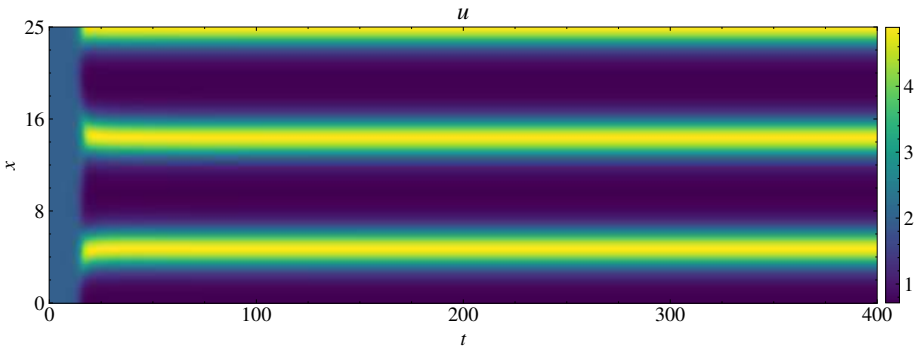

Figure 7: Numerical solution of the Brusselator exhibiting a Turing instability on a fixed domain of $L = 25$ with parameter values $(D, a, b) = (20, 2, 3)$. Here the dominant wave mode is $n = 5$.

References

[1] U. M. Ascher, S. J. Ruuth, and B. T. R. Wetton. "Implicit-Explicit Methods for Time-Dependent Partial Differential Equations". In: *SIAM Journal on Numerical Analysis* 32.3 (June 1995), pp. 797–823. ISSN: 1095-7170. DOI: 10.1137/0732037.

[2] C. H. L. Beentjes. *Pattern Formation Analysis in the Schnakenberg Model*. Tech. rep. University of Oxford, UK, 2015.

[3] A. R. Champneys et al. "Bistability, Wave Pinning and Localisation in Natural Reaction–Diffusion Systems". In: *Physica D: Nonlinear Phenomena* 416 (Feb. 2021), p. 132735. ISSN: 0167-2789. DOI: 10.1016/j.physd.2020.132735.

[4] E. Crampin, E. A. Gaffney, and P. K. Maini. "Reaction and Diffusion on Growing Domains: Scenarios for Robust Pattern Formation". In: *Bulletin of Mathematical Biology* 61.6 (Oct. 1999), pp. 1093–1120. ISSN: 0092-8240. DOI: 10.1006/bulm.1999.0131.

[5] E. Crampin, W. W. Hackborn, and P. K. Maini. "Pattern Formation in Reaction–Diffusion Models with Nonuniform Domain Growth". In: *Bulletin of Mathematical Biology* 64.4 (July 2002), pp. 747–769. ISSN: 0092-8240. DOI: 10.1006/bulm.2002.0295.

[6] K. Gowda et al. "Assessing the Robustness of Spatial Pattern Sequences in a Dryland Vegetation Model". In: *Proceedings of the Royal Society A: Mathematical, Physical and Engineering Sciences* 472.2187 (Mar. 2016), p. 20150893. ISSN: 1471-2946. DOI: 10.1098/rspa.2015.0893.

[7] D. S. Grebenkov and B. T. Nguyen. "Geometrical Structure of Laplacian Eigenfunctions". In: *SIAM Review* 55.4 (Jan. 2013), pp. 601–667. ISSN: 1095-7200. DOI: 10.1137/120880173.

[8] P. Grindrod. *Patterns and Waves*. en. Oxford Applied Mathematics & Computing Science Series. Oxford, England: Clarendon Press, Sept. 1991.

[9] P. Hartman. "A Lemma in the Theory of Structural Stability of Differential Equations". In: *Proceedings of the American Mathematical Society* 11.4 (1960), pp. 610–620. ISSN: 1088-6826. DOI: 10.1090/s0002-9939-1960-0121542-7.

[10] B. S. Jovanović and E. Süli. *Analysis of Finite Difference Schemes: For Linear Partial Differential Equations with Generalized Solutions*. Springer London, 2014. ISBN: 9781447154600. DOI: 10.1007/978-1-4471-5460-0.

[11] A. L. Krause, E. A. Gaffney, and B. J. Walker. "Concentration-Dependent Domain Evolution in Reaction–Diffusion Systems". In: *Bulletin of Mathematical Biology* 85.2 (Jan. 2023). ISSN: 1522-9602. DOI: 10.1007/s11538-022-01115-2.

[12] P. M. Kulesa et al. "On a Model Mechanism for the Spatial Patterning of Teeth Primordia in the Alligator". In: *Journal of Theoretical Biology* 180.4 (June 1996), pp. 287–296. ISSN: 0022-5193. DOI: 10.1006/jtbi.1996.0103.

[13] I. Lengyel and I. R. Epstein. "The Chemistry Behind the First Experimental Chemical Examples of Turing Patterns". In: *Chemical Waves and Patterns*. Springer Netherlands, 1995, pp. 297–322. ISBN: 9789401111560. DOI: 10.1007/978-94-011-1156-0_9.

[14] A. Madzvamuse and P. K. Maini. "Velocity-Induced Numerical Solutions of Reaction-Diffusion Systems on Continuously Growing Domains". In: *Journal of Computational Physics* 225.1 (July 2007), pp. 100–119. ISSN: 0021-9991. DOI: 10.1016/j.jcp.2006.11.022.

[15] P. K. Maini and T. E. Woolley. "The Turing Model for Biological Pattern Formation". In: *Mathematics of Planet Earth*. Springer International Publishing, 2019, pp. 189–204. ISBN: 9783030225834. DOI: 10.1007/978-3-030-22583-4_7.

[16] T. Miura et al. "Mixed-Mode Pattern in Doublefoot Mutant Mouse Limb - Turing Reaction-Diffusion Model on a Growing Domain During Limb Development". In: *Journal of Theoretical Biology* 240.4 (June 2006), pp. 562–573. ISSN: 0022-5193. DOI: 10.1016/j.jtbi.2005.10.016.

[17] J. D. Murray. *Mathematical Biology II: Spatial Models and Biomedical Applications*. Vol. 18. Interdisciplinary Applied Mathematics. Springer New York, 2003. DOI: 10.1007/b98869.

[18] J.D. Murray. "Parameter Space for Turing Instability in Reaction Diffusion Mechanisms: A Comparison of Models". In: *Journal of Theoretical Biology* 98.1 (Sept. 1982), pp. 143–163. ISSN: 0022-5193. DOI: 10.1016/0022-5193(82)90063-7.

[19] Q. Ouyang and H. L. Swinney. "Transition From a Uniform State to Hexagonal and Striped Turing Patterns". In: *Nature* 352.6336 (Aug. 1991), pp. 610–612. ISSN: 1476-4687. DOI: 10.1038/352610a0.

[20] K. J. Painter, P. K. Maini, and H. G. Othmer. "Stripe Formation in Juvenile Pomacanthus Explained by a Generalized Turing Mechanism with Chemotaxis". In: *Proceedings of the National Academy of Sciences* 96.10 (May 1999), pp. 5549–5554. ISSN: 1091-6490. DOI: 10.1073/pnas.96.10.5549.

[21] I. Prigogine and G. Nicolis. "Self-Organisation in Nonequilibrium Systems: Towards A Dynamics of Complexity". In: *Bifurcation Analysis*. Springer Netherlands, 1985, pp. 3–12. ISBN: 9789400962392. DOI: 10.1007/978-94-009-6239-2_1.

[22] S. J. Ruuth. "Implicit-Explicit Methods for Reaction-Diffusion Problems in Pattern Formation". In: *Journal of Mathematical Biology* 34.2 (1995), pp. 148–176. ISSN: 1432-1416. DOI: 10.1007/bf00178771.

[23] J. Schnakenberg. "Simple Chemical Reaction Systems with Limit Cycle Behaviour". In: *Journal of Theoretical Biology* 81.3 (Dec. 1979), pp. 389–400. ISSN: 0022-5193. DOI: 10.1016/0022-5193(79)90042-0.

[24] D. C. Thorstenson and D. W. Pollock. "Gas Transport in Unsaturated Porous Media: The Adequacy of Fick's Law". In: *Reviews of Geophysics* 27.1 (Feb. 1989), pp. 61–78. ISSN: 1944-9208. DOI: 10.1029/rg027i001p00061.

[25] A.M. Turing. "The Chemical Basis of Morphogenesis". In: *Philosophical Transactions of the Royal Society of London. Series B, Biological Sciences* 237.641 (Aug. 1952), pp. 37–72. DOI: 10.1098/rstb.1952.0012.

[26] J. C. Tzou et al. "Homoclinic Snaking Near a Codimension-Two Turing-Hopf Bifurcation Point in the Brusselator Model". In: *Physical Review E* 87.2 (Feb. 2013). ISSN: 1550-2376. DOI: 10.1103/physreve.87.022908.

[27] M. Zhang et al. *Coupled Reaction-Diffusion Systems and 1-D Pattern Formation, Part III: Pattern Formation on a Growing Domain*. 2015. URL: https://mengsenz.github.io/presentations/NASC_GrowingDomain_final.pdf (visited on 12/15/2023).